

Bubble acceleration of electrons with few-cycle laser pulses

This article has been downloaded from IOPscience. Please scroll down to see the full text article.

2006 New J. Phys. 8 186

(<http://iopscience.iop.org/1367-2630/8/9/186>)

View [the table of contents for this issue](#), or go to the [journal homepage](#) for more

Download details:

IP Address: 130.183.91.154

The article was downloaded on 20/07/2010 at 08:42

Please note that [terms and conditions apply](#).

Bubble acceleration of electrons with few-cycle laser pulses

Michael Geissler¹, Jörg Schreiber and Jürgen Meyer-ter-Vehn

Max-Planck-Institut für Quantenoptik, Hans-Kopfermann-Str. 1,
D-85748 Garching, Germany
E-mail: michael.geissler@mpq.mpg.de

New Journal of Physics **8** (2006) 186

Received 4 May 2006

Published 12 September 2006

Online at <http://www.njp.org/>

doi:10.1088/1367-2630/8/9/186

Abstract. We present three-dimensional particle-in-cell (3D-PIC) simulations of laser wake field acceleration (LWFA) of electrons in the bubble regime, using the code ILLUMINATION. The study is motivated by the new Light Wave Synthesizer (LWS), currently under construction at Max-Planck-Institut für Quantenoptik (MPQ), which is expected to produce short (sub-10 fs), high power (multi-terawatt) laser pulses. They will be short enough for optimal drive of bubbles in dense gas jet targets at laser energies as low as 20 mJ and to generate efficiently very bright, quasi-monoenergetic, low-emittance bunches of 10–100 MeV electrons. It is shown how the results change when plasma density, laser amplitude and focusing are varied. The density and the spectral evolution of bubble evolution are presented for a reference case in much detail in terms of a [movie](#). In particular, the formation of peaked spectra with an energy spread in the range of 10% are discussed qualitatively. Also plasma dynamics at the laser front and the rear vertex of the bubble as well as the periodic structures in the stem of accelerated electrons are addressed.

¹ Author to whom any correspondence should be addressed.

Contents

1. Introduction	2
2. Three-dimensional particle-in-cell (3D-PIC) simulations with the code ILLUMINATION	3
3. Bubble formation	4
4. First stages of bubble formation	5
5. Spectral bunching	6
6. Details of laser electron expulsion and electron trapping	8
7. Wave breaking versus self-trapping	8
8. Changing laser amplitude and focus	9
9. Lower limit for bubble acceleration for 5 fs pulses	10
10. Conclusions and outlook	11
Acknowledgments	12
References	12

1. Introduction

Laser wake field acceleration (LWFA) is the most important concept of particle acceleration by laser pulse in dense plasma [1]. For ultra-short pulses interacting with gas jets, the laser pulse ionizes the gas and drives a plasma wave. This is illustrated in figure 1. At sufficiently high intensities, self-trapping of plasma electrons occurs and peaked spectra of accelerated electrons are found. This is the so-called bubble regime [2]. Here, we investigate threshold conditions for bubble formation, in particular in the context of 5 fs, multi-TW pulses. Since laser energy is the dominant parameter (which defines the laser cost) few cycle pulses are best adjusted to this acceleration regime. Corresponding lasers are now becoming available [3].

Bubble acceleration differs from traditional wake field acceleration in that one drives the plasma far beyond the wave-breaking limit, such that a single wake rather than a regular plasma wave train is formed. In this regime, large amounts of plasma electrons (in the order of nano-Coulombs) self-trap in the wake and are accelerated without interacting directly with the laser field. The bubble length is approximately one plasma wavelength λ_p , and an important condition to generate electron spectra peaked in energy is that the laser pulse extends over $\lambda_p/2$ or less. For longer pulses, the accelerating electrons interact directly with the laser pulse, and one obtains broad thermal-like spectral shapes, see e.g. [4].

Peaked electron spectra were detected in recent experiments [5]–[11]. For example, the electron beams obtained by Faure *et al* [7] with 1 J, 30 fs laser pulses, consisted of low-emittance, 0.5 nC, 170 MeV electron bunches, accelerated over distances of just 3 mm with 15% laser-to-electron conversion efficiency. Still these results came as a surprise, because in all the experiments performed so far the laser pulses were longer than $\lambda_p/2$. The reason why the bubble regime could be accessed nevertheless is that nonlinear laser plasma interaction tends to shape the incident laser pulses until they fit into the first wake and can produce mono-energetic pulses. Apparently, the bubble regime has the properties of an attractor. This is concluded from simulations presented in [7, 10]. The theory of bubble formation, its stability, and its scaling properties has been

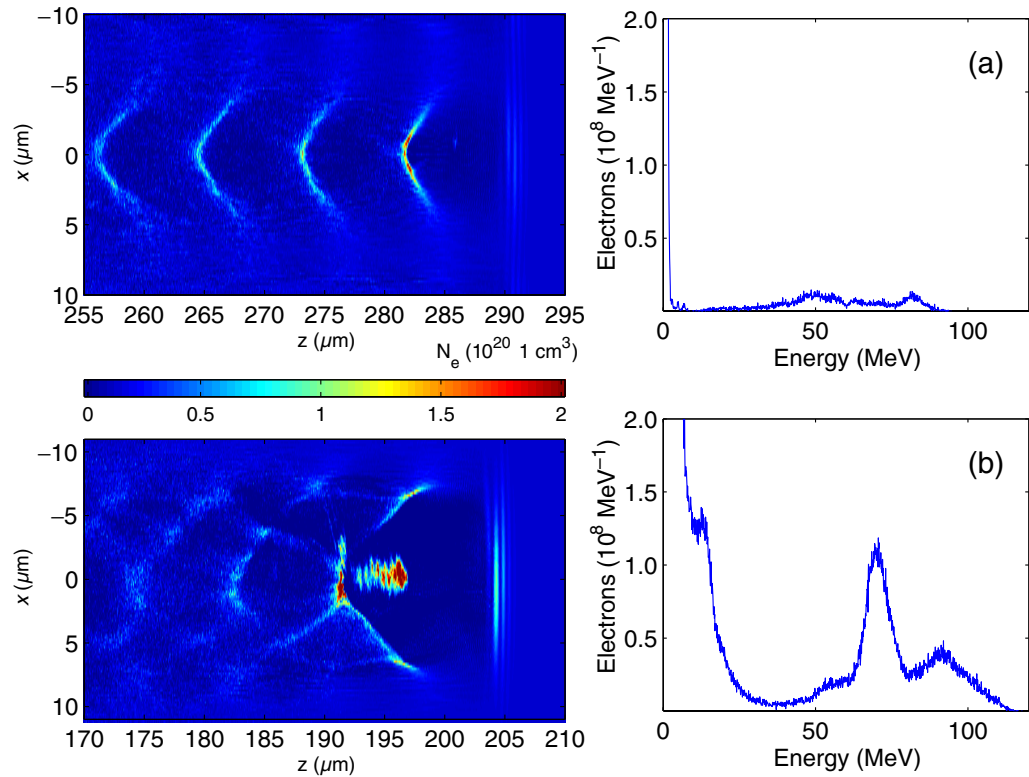


Figure 1. Snapshots of electron density and electron energy spectra for two different laser amplitudes: (a) $a_0 = 3$ (below bubble threshold) and (b) $a_0 = 5$ (above bubble threshold). For $a_0 = 5$, see also the [movie](#). In both cases, snapshots were taken at times when acceleration saturates and further propagation increases neither the maximum energy nor the position of the peak in the spectrum.

developed by Gordienko and Pukhov [12]. It applies to the ultra-relativistic regime, $a_0 \gg 1$. The present study primarily considers lower a_0 values, relevant in near-term experiments.

The advent of high-power few-cycle laser pulses makes it possible to drive bubble wake fields optimally adjusted to dense gas jet plasmas and to achieve stable acceleration. This is discussed in the present paper. After defining laser and plasma parameters in section 2, the threshold for bubble formation is explored in section 3. Then a reference case is discussed in much detail in sections 4–6, based on the accompanying [movie](#). Laser focus and intensity of the reference case are chosen in view of the upcoming experiments. Variations to higher intensities and smaller focal radii are addressed in section 8.

2. Three-dimensional particle-in-cell (3D-PIC) simulations with the code ILLUMINATION

The simulations are performed with the 3D-PIC code ILLUMINATION. The typical simulation box is $200 \times 200 \times 1000$ cells and has a volume of $38 \times 38 \times 50 \mu\text{m}^3$. Each cell contains one macro-particle corresponding to 40 million particles. The simulated box co-moves with the laser at the velocity of light to simulate only the laser plasma interaction region. The plasma is assumed

to be fully ionized with immobile ions as a neutralizing background. We have checked that allowing for ion motion gives almost the same results.

Throughout the paper the laser pulse is linear polarized in \vec{e}_x , propagate in \vec{e}_z and has a centre wavelength of $\lambda_0 = 800$ nm. The normalized vector potential of the incident laser pulse, $a = eA/mc^2$, depends on radius and time in the form

$$a(r, t) = a_0 \exp(-(r/w_0)^2) \exp(-2 \ln 2 (t/\tau_0)^2). \quad (1)$$

Here, e and m are charge and rest mass of electrons, and c is the velocity of light. For the reference pulse, we choose a focal radius of $w_0 = 5 \mu\text{m}$ and a full-width-at-half-maximum duration of the intensity of $\tau_0 = 5$ fs. This implies a Rayleigh length of $z_R = \pi w_0^2/\lambda_0 = 98 \mu\text{m}$. Further the intensity, the peak power, and the total pulse energy can be calculated as $I = 2.2 \times 10^{18} \text{ W cm}^{-2} \times a_0^2$, $P = \pi w_0^2 I/2$ and $W = 1.67 I \tau_0 w_0^2$, respectively.

The plasma electron density is chosen as $n_0 = 1.745 \times 10^{19} \text{ cm}^{-3}$, corresponding to 1% of the critical density for $\lambda_0 = 800$ nm light, $n_{\text{cr}}/n_0 = (\omega_0/\omega_p)^2 = 100$. This determines the group velocity of the laser pulse inside the plasma, which is equal to the phase velocity of the wake field, $\beta_{\text{ph}} = \sqrt{1 - (\omega_p/\omega_0)^2} \approx 0.995$, and leads to the wake field γ -factor of $\gamma_{\text{ph}} = (1 - \beta_{\text{ph}}^2)^{-1/2} = \omega_0/\omega_p = 10$. Here, $\omega_0 = 2\pi c/\lambda_0$ and $\omega_p = 4\pi e^2 n_0/m$ are laser and plasma frequency, respectively, and the plasma wavelength is $\lambda_p = 2\pi c/\omega_p = 8 \mu\text{m}$. At high laser intensities, these parameters will change due to relativistic increase of electron mass. Approximate expressions are obtained from $\omega_p^{\text{rel}} \approx \omega_p/\sqrt{\gamma_{\text{av}}}$, where the γ -factor averaged over the electron distribution is defined by $1/\gamma_{\text{av}} = \langle 1/\gamma \rangle$. For linear polarization, it depends on the laser amplitude approximately in the form $\gamma_{\text{av}} \approx \sqrt{1 + a_0^2/2}$.

3. Bubble formation

Figure 1 shows simulations for two different laser amplitudes. The upper frames correspond to $a_0 = 3$ (≈ 41 mJ) and the lower ones to $a_0 = 5$ (≈ 115 mJ). Both pulses are shorter than the length of the wake field and therefore fulfil the first condition for bubble acceleration. However, the second one of achieving self-trapping of ambient plasma electrons in the first wake is satisfied for $a_0 = 5$ only. This is evident from the density plots on the left side of figure 1.

In the first case, a highly nonlinear, but still regular plasma wave is seen in the density plot, trailing the short laser pulse (not shown explicitly). The high-density crests of the wave are curved due to relativistic and other nonlinear effects, but still only a relatively small number of electrons (in the order of 10^7 MeV^{-1}) is trapped in the low-density wave buckets and accelerated to energies of 40–80 MeV. This changes drastically when raising a_0 from 3 to 5. Then the pattern of the regular wave train disappears, and a high-density stem of accelerated electrons shows up in the first wake bucket behind the laser pulse. One should notice that the regular wave crests in figure 1(a) are separated by the plasma wavelength of about $8 \mu\text{m}$. This changes due to charge loading in figure 1(b). The length of the first wake, the *bubble*, increases, while the downstream wave pattern is increasingly broken and washed out.

After a certain propagation distance, a peak appears in the energy spectrum of the trapped electrons. In figure 1(b), it is seen at 70 ± 5 MeV after $200 \mu\text{m}$ of propagation. The total number and energy of accelerated electrons contained in this peak (> 60 MeV) is plotted in figure 2 as a function of time together with the laser energy. One observes that the peak starts to build

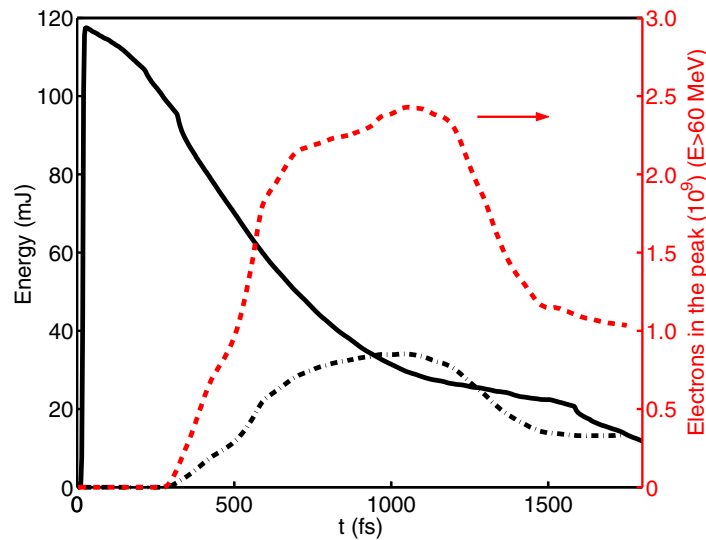


Figure 2. Number (red dashed) and total energy (black dashed-dotted) of electrons with particle energy >60 MeV as a function of time; also shown is energy in the laser pulse (black full).

up after 300 fs ($z = 100 \mu\text{m}$) and to saturate after 600 fs ($z = 200 \mu\text{m}$), when the number of electrons above 60 MeV approaches 2×10^9 . At this time, the total energy in the electron peak is roughly 30 mJ, which amounts to 25% of the incident laser energy. In the subsequent evolution, number and energy of peak electrons still increase somewhat, until the peak decays after 1200 fs ($z = 400 \mu\text{m}$).

4. First stages of bubble formation

Details of bubble evolution are presented in the following by means of the [movie](#). At time $t = 0$ fs, the centre of the laser pulse is located at $z = -10 \mu\text{m}$, moving to the right. After 30 fs, the pulse starts to touch the plasma density profile, which rises in a linear ramp ($z = 0-10 \mu\text{m}$) to the value of $1.745 \times 10^{19} \text{cm}^{-3}$. At 90 fs, the formation of the first wake bucket is almost complete. The imprint of laser action is seen on the right side in the form of vertical high-density layers, separated by half the laser wavelength. These layers correspond to electrons trapped between the peaks of laser intensity. They are expelled mainly in the transverse direction. After expulsion they swing back to the laser axis. In the ramp region, this radially converging flow has already formed a high density spot on the axis. After 100 fs, bubble formation is complete. At this time, the longitudinal bubble extension is $\lambda_{\text{bub}} \approx 11 \mu\text{m}$, somewhat longer than the plasma wavelength $\lambda_p = c/\omega_p = 8 \mu\text{m}$. This is expected due to the relativistic reduction of ω_p . From $\lambda_{\text{bub}}/\lambda_p \approx \sqrt{\gamma_{\text{av}}}$, we obtain $\gamma_{\text{av}} \approx 2$; here $1/\gamma_{\text{av}} = \langle 1/\gamma \rangle$ defines the average taken over the laser-excited electrons involved in the bubble dynamics. At 115 fs, the laser pulse approaches the right border of the simulation box, and now cells are added at this border and dropped at the left border to follow pulse propagation through undisturbed plasma.

Between 100 and 150 fs, a rather regular bubble is seen. It is practically void of electrons, while ions are nearly unperturbed and create a high, mainly longitudinal E-field. The most

conspicuous feature is observed at the rear vertex, where electrons accumulate and create a region of high space charge. A portion of the electrons coming in radially is scattered into the bubble and starts to be accelerated in the wake field. During the time period of 150 to 350 fs, the accelerated electrons generate a plateau-like spectrum between 10 and 50 MeV and form a narrow stem along the bubble axis.

The distance between the base of the stem and the peak of the laser pulse is about $11 \mu\text{m}$ at 100 fs and lengthens to $14 \mu\text{m}$ at 150 fs. This gradual lengthening is attributed to the effect of beam loading. At this time, the number of trapped electrons has reached about 2×10^9 . Electron trapping then drops sharply. Beam loading also changes the shape of the bubble near the vertex from spherical at 100 fs to conical at 150 fs. Details of vertex and stem structure will be discussed further below.

5. Spectral bunching

An important feature of bubble acceleration is that it leads to relatively sharp peaks in the electron energy spectra during later phases of spectral evolution. In the reference case presented in the [movie](#), this happens during 350 and 700 fs. At 350 fs, the plateau-like spectrum is divided into a front sector (40–60 MeV), which mainly contains electrons trapped close to the plasma surface in the initial phase of bubble formation, and a second sector (10–40 MeV), from which the spectral peak develops over the next 200 fs. At 700 fs, a sharp peak at $70 \pm 5 \text{ MeV}$ has formed. It sits on top of a broader spectrum extending to somewhat above 100 MeV. This spectral pattern stays almost invariant until 800 fs. It then broadens and decays, and also the bubble as a whole starts to degrade. The main reason for this is depletion of laser energy and that the laser pulse has passed the focal volume ($z = 0\text{--}100 \mu\text{m}$) and widens again.

In order to better understand the reason for the spectral bunching, we show in [figure 3](#) the trajectories of all electrons that reach energies between 60 and 80 MeV after 700 fs. These are the electrons forming the sharp peak in [figure 1](#). We have plotted energy versus spatial coordinates x (laser-polarization direction) and z (laser-propagation direction). It is seen that all the electrons producing the quasi-mono-energetic peak originate from the first $80 \mu\text{m}$ of the plasma volume. They were trapped in the time interval of 0–350 fs. They are then accelerated over a distance of $100\text{--}120 \mu\text{m}$ and reach peak energies of 60–100 MeV at times of 700–800 fs (see [movie](#)). The acceleration distance is considerably smaller than the dephasing length $L_d = \lambda_d \gamma_{\text{ph}}^2 \approx 800 \mu\text{m}$; rather than by dephasing it is determined by depletion of laser energy. According to the general analysis of Gordienko and Pukhov [12], this is typical for the bubble regime.

Still we need to understand what determines the formation of the spectral peak at later times. The most immediate explanation is that the electrons in the peak have passed approximately the same electric potential. This is indeed expected for the group of electrons that is trapped after 100 fs, when the bubble has formed and is propagating in a stationary fashion. Trapping stops at 350 fs, and the acceleration for each group of trapped electrons takes about 300–350 fs. Therefore this regular phase of acceleration terminates at 700 fs. The spread of the energy peak may be explained by the fact that the laser energy already decays during this time (to 50% at 700 fs, see [figure 2](#)), and the bubble acceleration field decreases correspondingly.

The insert in [figure 3](#) provides some more details about the energy bunching in the present simulation. It shows the trajectories projected into the $x = 0$ plane and plotted in terms of number density in grey-scale. Careful inspection indicates that electrons trapped late experience

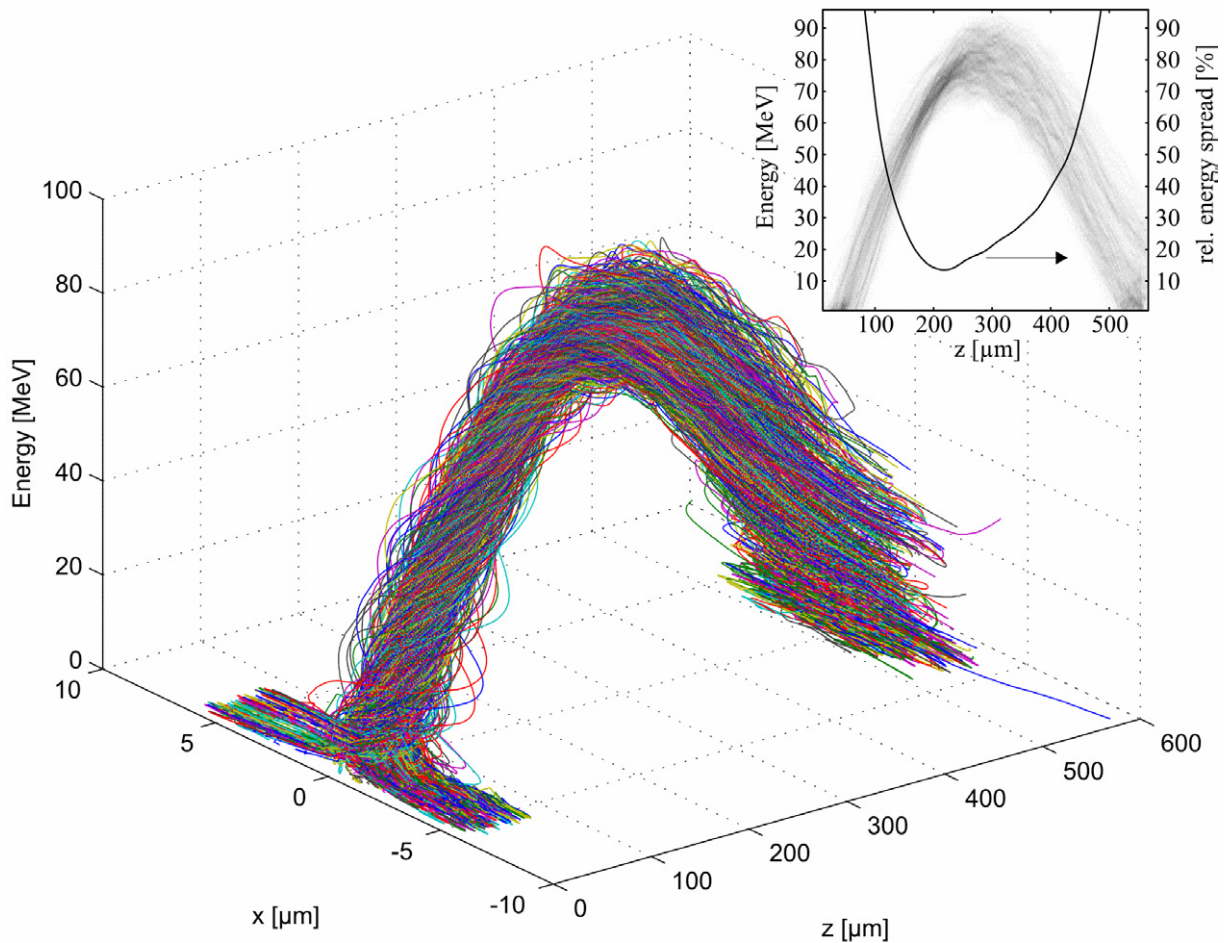


Figure 3. Trajectories of trapped electrons reaching energies > 60 MeV (those included in figure 2). The perspective view shows particle energy versus x and z (laboratory) coordinates. The insert shows the main plot projected into the E , z plane; instead of single trajectories, electron density (trajectory number per z interval) is given in grey scale. Also the relative energy spread is given as the solid curve.

a somewhat higher acceleration field than those trapped early. This adds to the energy focusing in the region around $z = 200 \mu\text{m}$. The relative energy spread is also given in the insert. It falls to 10–15% in this region. For reducing the energy spread, one would have to reduce the time interval in which electrons are injected into the bubble. The injection problem has been discussed in more detail by van der Wiel *et al* [13]. We also refer to Bulanov *et al* [14] for an approximate analytical description of the spectral evolution.

For making use of the mono-energetic bunch in the present simulation, one would have to extract it from the plasma in time. For this it is best to cut the plasma layer at 200–250 μm and to release the bunch into vacuum at this distance. New methods of how to produce such ultra-thin gas jet layers are currently under investigation [15]. For thicker gas jets, one should shift the laser focus to the rear side of the jet. We have checked that laser pulse propagation through plasma in front of the focus does not significantly change the results seen in the [movie](#). On the other hand,

the accelerated electron bunch degrades rapidly when propagating inside the plasma behind the focal region. This is seen in the [movie](#). When the laser pulse loses its function as bubble driver, the electron bunch takes over the role of the driving pulse, and a secondary electron-driven cavity is formed. This is observed in the later stages of the [movie](#) between 800 and 1300 fs. A recent discussion on driving wake fields with electron pulses was given by Joshi and Mori [16].

6. Details of laser electron expulsion and electron trapping

Here, we discuss some finer details observed in the [movie](#).

1. At the front side of the bubble in the laser interaction region.
2. At the rear side in the vertex region.
3. The oscillatory structure in the stem of trapped electrons.

The laser action on the plasma is often viewed as a snowplough, piling up electrons at the front which are then pushed in transverse direction by the ponderomotive force. Here, we observe that the electrons are first trapped in the ponderomotive buckets of the laser wave, forming electron layers separated by half the laser wavelength. Due to the high electron density, the wavelength appears to be about 10–20% longer than $\lambda_0/2$. The electrons are then radially expelled from these layers. Due to the linear polarization in the x, z plane, the distribution of the expelled electrons shows some azimuthal variations, but on the average they form the surface of an axially symmetric bubble, dragged by the laser pulse to the right.

The details of the 3D electron trajectories are quite complex and cannot be followed in the x, z cut of the [movie](#). Nevertheless, one can observe that the electron flow along the bubble surface is not completely uniform, but carries the imprint of the spatially structured expulsion on the laser side. The electrons coming in radially at the vertex and being trapped and accelerated in the stem appear in bunches forming the oscillatory structure in the stem. The period of this structure is 0.45–0.50 μm , close to the period observed on the laser side. Direct laser action on the stem appears to be too weak to explain the structure.

7. Wave breaking versus self-trapping

A characteristic feature of the bubble regime is the very efficient self-trapping of background electrons. This is often referred to as wave breaking, but it is important to understand that self-trapping occurring in the 3D bubble regime is quite different from the wave breaking of 1D plasma waves [17, 18]. In 1D geometry, breaking of laser-driven plasma waves sets in for $a_0 > 2(\omega_0/\omega_p)^{2/3}$ (see Bulanov [14], here given for linear polarization).

For the present value of $\omega_0/\omega_p = 10$, this condition is neither met by $a_0 = 3$ nor $a_0 = 5$. Nevertheless, very efficient electron trapping in the wake is observed for $a_0 = 5$. This is attributed to the fact that electron motion close to the vertex is transverse rather than longitudinal. The curved plasma wave fronts lead to transverse wave breaking [18] occurring for reduced threshold values; it also generates the swallow-tail density structures behind the vertex, clearly seen in figure 1 and the [movie](#).

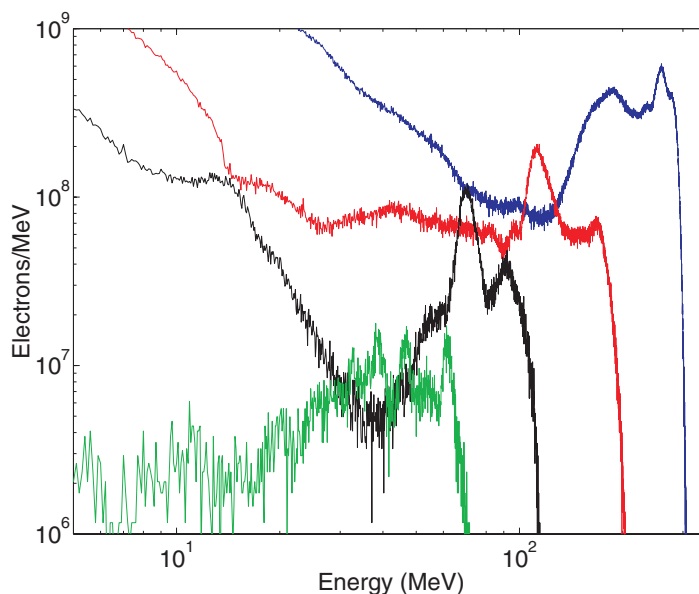


Figure 4. Spectra of accelerated electrons for different laser amplitudes a_0 , while the other parameters $w_0 = 5 \mu\text{m}$, $\tau = 5 \text{fs}$ and $n_0 = 1.745 \times 10^{19} \text{cm}^{-3}$ are the same as in the reference case. Green: $a_0 = 3$ (after $300 \mu\text{m}$), black: $a_0 = 5$ (after $220 \mu\text{m}$), red: $a_0 = 10$ (after $250 \mu\text{m}$), blue: $a_0 = 30$ (after $550 \mu\text{m}$). As in figure 1, the corresponding propagation distances mark the acceleration length where the peak in the electron spectrum reaches the highest energy.

For fully developed bubbles at even higher laser intensities, these structures also disappear, the downstream electron flow becomes completely turbulent, and the electron distribution function close to the vertex is thermal-like, different from the multi-fluid flow characteristic for wave breaking. Strictly speaking, there is no wave breaking at all during particle trapping. This was clearly pointed out by Gordienko and Pukhov [12]. Wave breaking in the sense of multi-velocity flow only occurs at later times during the decay of the bubble. The scattering of radially inflowing electrons by the vertex potential, either downstream into the breakwaters or upstream to feed the stem, was described by Kostyukov *et al* [19].

8. Changing laser amplitude and focus

Here we add results on electron spectra when changing a_0 between 3 and 30, keeping the parameters $w_0 = 5 \mu\text{m}$, $\tau = 5 \text{fs}$ and $n_0 = 1.745 \times 10^{19} \text{cm}^{-3}$ fixed. The spectra obtained for $a_0 = 3, 5, 10, 30$, are plotted in figure 4. For $a_0 = 5, 10, 30$, they have similar shapes. The spectra are taken at distances l_{acc} , at which the energy E_{peak} of the peak in the spectrum reaches the highest value. Propagation beyond this acceleration length leads to rapid degradation of the peak.

The key parameters from this set of simulations are summarized in table 1. The acceleration length and the peak electric field scale approximately like $l_{\text{acc}} \propto \sqrt{a_0}$ and $\mathcal{E}_z \propto a_0^{0.25}$, and the peak energy follows $E_{\text{peak}} \approx 0.3\mathcal{E}_z l_{\text{acc}}$. We have then also varied the laser spot radius w_0 . For the bubble radius we find $R_b \approx w_0 a_0^{0.25}$ and for the acceleration length $l_{\text{acc}}(\mu\text{m}) \approx 40\sqrt{a_0 w_0}(\mu\text{m})$.

Table 1. Key parameters for different a_0 as presented in figure 4. \mathcal{E}_z is the peak of the acceleration field at the bubble boundary, $N_{e,\text{peak}}$ is the number of electrons forming the peak after l_{acc} , and W_{peak} is the spectral energy of the peak. The numbers in parentheses are obtained from self-similarity theory

a_0	W_{Laser} (mJ)	l_{acc} (μm)	\mathcal{E}_z (TV/m)	N_{peak} (10^9)	E_{peak} (MeV)	W_{peak} (mJ)
5	115	220 (92)	1.1 (0.94)	1.2 (1.6)	70 (18)	14
10	460	250 (183)	1.6 (1.33)	3.8 (4.6)	130 (52)	75
30	4140	550 (550)	2.3 (2.3)	24 (24)	270 (270)	1300

Combining results and making use of $\mathcal{E}_z \propto n_0 R_b$, we obtain for the peak energy as a function of the external parameters, plasma density n_0 , laser amplitude a_0 , and focus radius w_0 ,

$$E_{\text{peak}}(\text{MeV}) \approx n_0 [10^{19} \text{cm}^{-3}] (w_0(\mu\text{m}))^{1.5} a_0^{0.75}, \quad (2)$$

This formula is in reasonable agreement with the simulation results. Here, one should keep in mind, however, that w_0 and n_0 cannot be varied independently over a larger range. In order to stay in the stable bubble regime, one has to match the plasma wavelength λ_p roughly with bubble diameter:

$$\lambda_p \approx 2R_b = 2w_0 a_0^{0.25} \quad (3)$$

Always assuming that the laser pulse is shorter than λ_p , the bubble diameter can be slightly tuned by laser intensity, once the plasma density is chosen, but has to stay in the range of λ_p . Expressing it in more experimental terms, for a given laser pulse, there exists a small density window for bubble acceleration.

It is interesting to compare the present results with the scaling relations derived by Gordienko and Pukhov [12]. Their central observation is that, in the ultra-relativistic regime ($a_0 \gg 1$), laser plasma dynamics evolves in a self-similar way when keeping $S = n_0 / (a_0 n_{\text{cr}}) = (\omega_p / \omega_0)^2 / a_0$ constant. This means one compares situations of same relativistic plasma frequency. This relativistic similarity is well confirmed by simulations [12]. When changing a_0 at constant n_0 , also $S \propto a_0^{-1}$ changes. For this case, the following scaling relations are given in [12]: transverse bubble radius $R \propto S^{-1/2} \propto a_0^{1/2}$, bubble acceleration field $\mathcal{E}_z \propto n_0 R \propto a_0^{1/2}$, acceleration length $l_{\text{acc}} \propto S^{-3/2} (c\tau_0 / R) \propto a_0$, peak electron energy $E_{\text{peak}} \propto \mathcal{E}_z l_{\text{acc}} \propto a_0^{3/2}$, peak electron number $N_{e,\text{peak}} \propto n_0 R^3 \propto a_0^{3/2}$. In table 1, numbers obtained from these relations are given in brackets. In view of the asymptotic character of these scalings $a_0 \gg 1$, we have normalized to values at $a_0 = 30$. While results for \mathcal{E}_z and $N_{e,\text{peak}}$ compare reasonably with the present simulations, acceleration length l_{acc} and peak energy E_{peak} scale much less with a_0 in the present simulations.

9. Lower limit for bubble acceleration for 5 fs pulses

Finally we address the question of to what extent bubble dimensions and required energy can be even further reduced, keeping the amplitude of the 5 fs laser pulse at the reference value

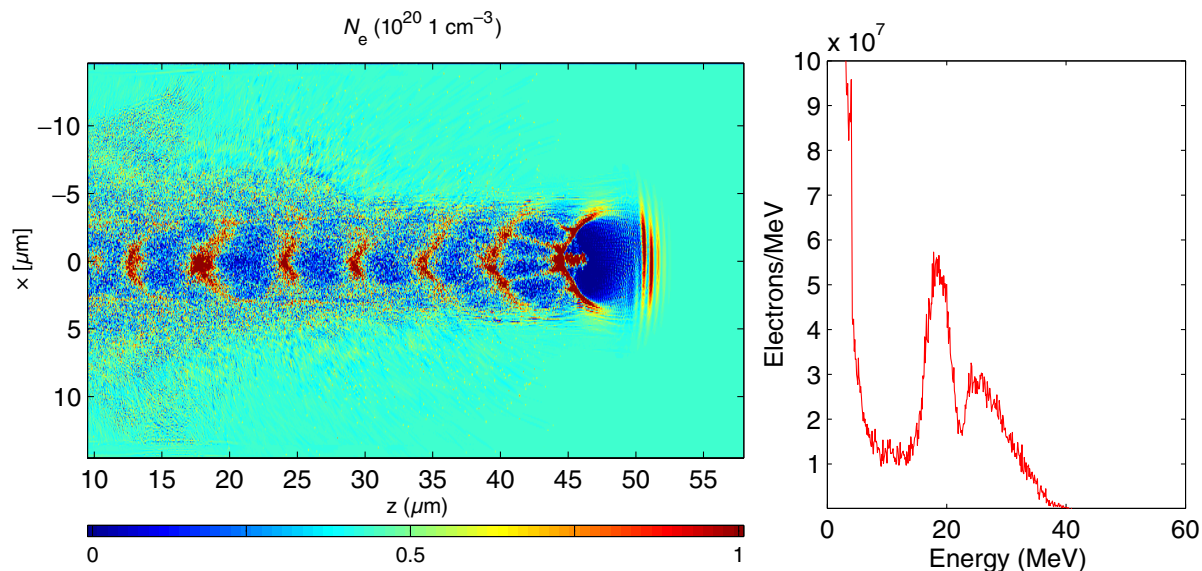


Figure 5. Electron density and spectrum for a 20 mJ laser propagating through a plasma with $\lambda_p = 5 \mu\text{m}$

of $a_0 = 5$ and satisfying condition (3) to warrant stable bubble formation. First we focus the beam to $w_0 = 2 \mu\text{m}$ rather than $w_0 = 5 \mu\text{m}$, thereby reducing the laser energy from 115 to 18.4 mJ, and then we choose $\lambda_p = 5 \mu\text{m}$, consistent with condition (3) and corresponding to $n_0 \approx 4.5 \times 10^{19} \text{ cm}^{-3}$.

Results obtained with these parameters are shown in figure 5 as a snapshot after $\approx 50 \mu\text{m}$ propagation. They should be compared with the reference case in figure 1. Again we observe a bubble with a stem of accelerating electrons. The peak in the spectrum is located at 20 MeV and contains $N_{\text{peak}} = 3.5 \times 10^8$ electrons and a total energy of $W_{\text{peak}} = 1 \text{ mJ}$. There are differences, however, when following this case for longer times. Although the bubble remains stable over $\approx 100 \mu\text{m}$, the spectrum rapidly changes, e.g. the peak observed at 20 MeV in figure 5 splits into two broader peaks at 25 and 40 MeV after $70 \mu\text{m}$; the spectral range between 10 and 60 MeV then contains 6×10^8 electrons and a total energy of 3 mJ. After $\approx 100 \mu\text{m}$, the bubble starts to decay due to laser depletion. The estimations of acceleration length and peak energy peak (equation (2)) apply to this phase. They give $l_{\text{acc}} \approx 125 \mu\text{m}$ and $E_{\text{peak}} = 42 \text{ MeV}$ which are in good agreement with the simulation.

This parameter set gives more or less the lower limit for bubble acceleration in terms of laser pulse energy. The bubble dimensions are close to the laser wavelength and cannot be further decreased. Decreasing the laser intensity would quickly lead to the breakdown of the bubble regime.

10. Conclusions and outlook

We have investigated bubble acceleration with few-cycle TW-to-PW laser pulses in view of experiments coming up in the near future. Based on 3D-PIC simulations, we have emphasized issues of immediate interest to experimentalists, such as the minimum requirements in laser

intensity and energy for reaching the bubble regime and peaked electron spectra with 5 fs pulses. Presenting a [movie](#) of a reference case, we also provide much more detailed information than has been published so far. This includes the late phases of laser depletion and bubble decay. A critical issue is to extract the pulse, when it has an optimal spectrum, and this requires ultra-thin gas jet layers, at least for the few-cycle laser pulses considered here. These pulses are optimally adjusted to drive wake field acceleration in the bubble regime at pulse energies in the milli-joule range which allows for table-top devices and high repetition rate. The fully self-organizing acceleration regime is remarkably stable, energy-efficient, and simple to install. It is therefore very attractive for many applications.

The simulations presented here show that peaked energy spectra can be obtained with an energy spread of about 10%. The energy width is related to the characteristics of electron self-trapping and laser energy depletion in the bubble regime. Of course, for certain applications, one would like to have much sharper energy spectra. For this goal, one has to control the process of feeding electrons into the wake field. One way would be to work at lower wake amplitudes, below the self-trapping limit, and to use either external injection or interaction with a second laser pulse [13, 20, 21]. It has still to be demonstrated that sufficient amounts of electrons in controlled space-time volumes can be generated in this way to achieve narrow energy spectra.

In principle, the bubble regime can be scaled to high particle energies, far above the GeV level [12]. This would imply, however, larger bubble volumes and, correspondingly, larger laser drive energies. Given the highly nonlinear character of this regime, in which all parameters are tightly interlinked with each other, bubble acceleration appears somewhat inflexible when trying to optimize particular parameters, in particular to reach GeV energies. A way to overcome these limitations may be staged acceleration, taking the bubble regime as an electron source producing nano-Coulombs of 10–1000 MeV electron bunches efficiently, and then to use either preformed laser plasma channels [22] to increase the acceleration length or vacuum laser acceleration schemes [23]. The vision is to create multi-GeV and TeV beams in this way.

Acknowledgments

This work was supported by DFG-Project Transregio TR18 and in part by the European Community within the framework of the Association EURATOM—Max-Planck-Institut für Plasmaphysik. MG is supported by the Austrian Academy of Sciences, APART Grant.

References

- [1] Esarey E, Sprangle P, Krall J and Ting A 1996 *IEEE Trans. Plasma Sci.* **24** 252
- [2] Pukhov A and Meyer-ter-Vehn J 2002 *Appl. Phys. B* **74** 355
- [3] Ishi N *et al* 2005 *Opt. Lett.* **30** 567
- [4] Gahn C, Tsakiris G D, Pukhov A, Meyer-ter-Vehn J, Pretzler G, Thierolf P, Habs D and Witte K J 1999 *Phys. Rev. Lett.* **83** 4772
- [5] Mangles S P D *et al* 2004 *Nature* **431** 535
- [6] Geddes C G R, Toth C, Tilborg J V, Esarey E, Schroeder C B, Bruhwilder D, Nieter C, Cary J and Leemans W P 2004 *Nature* **431** 538
- [7] Faure J, Glinec Y, Pukhov A, Kiselev S, Gordienko S, Lefebvre E, Rousseau J P, Burgy F and Malka V 2004 *Nature* **431** 541
- [8] Miura E *et al* 2005 *Appl. Phys. Lett.* **86** 251501

- [9] Yamazaki A *et al* 2005 *Phys. Plasmas* **12** 093101
- [10] Hidding B *et al* 2006 *Phys. Rev. Lett.* **96** 105004
- [11] Krushelnik K *et al* 2005 *Phys. Plasmas* **12** 056711
- [12] Gordienko S and Pukhov A 2005 *Phys. Plasmas* **12** 043109
Pukhov A and Gordienko S 2006 *Phil. Trans. R. Soc. A* **364** 623
- [13] van der Wiel M J, Lutten O J, Brussard G J H, van der Geer S B, Urbanus W H, van Dijk W and van Oudheusden Th 2006 *Phil. Trans. R. Soc. A* **364** 679
- [14] Bulanov S V, Yamagiwa M, Esirkepov T Zh, Koga J K, Kando M, Ueshima Y and Saito K 2005 *Phys. Plasmas* **12** 073103
- [15] Pai C-H, Huang S-Y, Kuo C-C, Lin M-W, Wang J, Chen S-Y, Lee C-H and Lin J-Y 2005 *Phys. Plasmas* **12** 070707
Hsieh C T, Huang C M, Chang C L, Ho Y C, Chen Y S, Lin J Y, Wang J and Chen S Y 2006 *Phys. Rev. Lett.* **96** 095001
- [16] Joshi C and Mori W B 2006 *Phil. Trans. R. Soc. A* **364** 577
- [17] Achiezer A I and Polovin R V 1956 *Sov. Phys.—JETP* **3** 696
- [18] Bulanov S V, Pegoraro F, Pukhov A M and Sakharov A S 1997 *Phys. Rev. Lett.* **78** 4205
Bulanov S V, Pegoraro F and Pukhov A M 1995 *Phys. Rev. Lett.* **74** 710
- [19] Kostyukov I, Pukhov A and Kiselev S 2004 *Phys. Plasmas* **11** 5256
- [20] Umstadter D, Kim J K and Dodd E 1996 *Phys. Rev. Lett.* **76** 2073
- [21] Esarey E *et al* 1997 *Phys. Rev. Lett.* **79** 2682
- [22] Leemans W, Esarey E, Geddes C, Schroeder C and Toth C 2006 *Phil. Trans. R. Soc. A* **364** 585
- [23] Malka V, Faure J, Glinec Y and Lifschitz A F 2006 *Phil. Trans. R. Soc. A* **364** 601